Available online at www.sciencedirect.com
ScienceDirect
Journal of Power Sources 159 (2006) 1458–1463
JOURNAL OF POWER SOURCES
www.elsevier.com/locate/jpowsour

Electrochemical properties of amorphous and icosahedral quasicrystalline $Ti_{45}Zr_{35}Ni_{17}Cu_3$ powders

Baozhong Liu [a,b], Yaoming Wu [a], Limin Wang [a,*]

[a] *Key Laboratory of Rare Earth Chemistry and Physics, Changchun Institute of Applied Chemistry, CAS, 5625 Renmin Street, Changchun 130022, China*
[b] *Graduate School of the Chinese Academy of Sciences, 19 Yuquan Road, Beijing 100049, China*

Received 21 September 2005; received in revised form 16 November 2005; accepted 23 November 2005
Available online 6 January 2006

Abstract

$Ti_{45}Zr_{35}Ni_{17}Cu_3$ amorphous and single icosahedral quasicrystalline powders were synthesized by mechanical alloying and subsequent annealing at 855 K. Microstructure and electrochemical properties of two alloy electrodes were characterized. When the temperature was enhanced from 303 to 343 K, the maximum discharge capacities increased from 86 to 329 mAh g^{-1} and 76 to 312 mAh g^{-1} for the amorphous and quasicrystalline alloy electrodes, respectively. Discharge capacities of two electrodes decrease distinctly with increasing cycle number. The I-phase is stable during charge/discharge cycles, and the main factors for its discharge capacity loss are the increase of the charge-transfer resistance and the pulverization of alloy particles. Besides the factors mentioned above, the formation of TiH_2 and ZrH_2 hydrides is another primary reason for the discharge capacity loss of the amorphous alloy electrode.

Keywords: Ti–Zr–Ni–Cu alloy; Amorphous; Icosahedral quasicrystal; Electrochemical properties; Mechanical alloying

1. Introduction

Hydrogen storage alloys have attracted much attention because they have wide applications, such as heat pump, secondary battery, isotopic separation, etc. [1]. Icosahedral quasicrystalline phase (I-phase) exhibits excellent hydrogen storage property because of the special crystal structure. Zn-based [2], Ti-based [3,4] and Zr-based [5,6] I-phase alloys have been widely investigated for their potential use.

Ti-based I-phase alloy becomes one of the most promising hydrogen storage materials due to thermodynamical stability, low cost and high hydrogen capacity. Stroud et al. [7] have firstly reported the hydrogen storage properties of Ti–Zr–Ni I-phase in 1996. The desorption of hydrogen from a $Ti_{45}Zr_{38}Ni_{17}$–H quasicrystal was observed by high-temperature X-ray powder diffraction, demonstrating a potential utility of Ti-based I-phase alloy. $Ti_{45}Zr_{38}Ni_{17}$ I-phase absorbed large amounts of hydrogen up to two hydrogen atoms per metal atom. Its loading capacity was higher than that of $LaNi_5$ and TiFe compounds, but the equilibrium plateau pressures were too low for gas storage applications [8]. In order to improve the ability of the hydrogen storage, Takasaki et al. [9] have prepared the quasicrystalline $Ti_{45}Zr_{38}Ni_{17}$ powder by mechanical alloying and subsequent annealing. The maximum absorbing capacity with an atom ratio of hydrogen to metal ([H]/[M]) is 1.5, which may be due to a small amount of the Ti_2Ni-type crystal phase in I-phase alloy. During hydrogen cycling (repeated absorption–desorption of hydrogen), the $Ti_{45}Zr_{38}Ni_{17}$ I-phase was not stable. Majzoub et al. [10] have reported the hydrogen to metal atom ratio of 1.9 was obtained without crystal hydride formation when electrochemical method was used to hydrogenate $Ti_{45}Zr_{38}Ni_{17}$ I-phase alloy. However, to date, only a few investigations have dealt with the electrochemical characteristics of I-phase alloy as negative material of nickel–metal hydride (Ni–MH) battery.

The formation of Ti–Zr–Ni–Cu amorphous and I-phase alloys has been reported in our previous work. We have examined the composition dependence of the structure as well as I-phase forming ability [11–13]. An improvement in the forming abilities of amorphous and I-phase has been obtained by adding Cu. In this study, $Ti_{45}Zr_{35}Ni_{17}Cu_3$ amorphous and single I-phase

* Corresponding author. Tel.: +86 431 5262447; fax: +86 431 5262447.
E-mail address: lmwang@ciac.jl.cn (L. Wang).

0378-7753/$ – see front matter © 2005 Elsevier B.V. All rights reserved.
doi:10.1016/j.jpowsour.2005.11.077

powders were synthesized by mechanical alloying and subsequent annealing at 855 K. Discharge capacities, cycle stabilities and the mechanism of the discharge capacity loss for two alloys were investigated in detail.

2. Experimental procedures

Elemental powders of Ti (100 mesh, 99.9%), Zr (100 mesh, 99.9%), Ni (150 mesh, 99.9%) and Cu (250 mesh, 99.99%) were used as starting materials in this study. A powder mixture with a desired composition of $Ti_{45}Zr_{35}Ni_{17}Cu_3$ was poured into the milling container. Mechanical alloying was carried out in a vibratory ball miller under the vibration frequency of 25 Hz and amplitude of 2.5 mm for 280 h in an argon atmosphere. The alloyed powders were sealed under dynamic vacuum ($<10^{-1}$ Pa) in a fused silica tube, and then annealed at 855 K for 30 min.

The pressure-composition isotherms (PCT) curves of the mechanical alloyed and annealed powders were measured by a Gas Reaction Controller at 523 K, and the charge/discharge properties were investigated by using an electrochemical charge/discharge method. Test electrodes were fabricated by compressing a mixture of 0.15 g alloy (200–400 mesh) and 0.75 g nickel carbonyl powder into a pellet of 10 mm in diameter under a pressure of 15 MPa. In order to perform XRD analysis of the MH powders after cycling, working electrodes composed of 0.5 g alloy powder with 0.1 g carbon and graphite. After different cycles, the pellet was crushed in air and rinsed with water. Electrochemical measurements were performed in a standard open three-electrode cell that consisted of a working electrode (metal hydride electrode), a counter electrode ($Ni(OH)_2$/NiOOH electrode), and a reference electrode (Hg/HgO electrode). The electrolyte in the cell was a 6 M KOH aqueous solution. Charge/discharge tests were carried out on an automatic galvanostatic system (DC-5). Each electrode was charged for 10 h at 60 mA g^{-1} and discharged to −0.6 V versus Hg/HgO at 30 mA g^{-1} at different temperatures (303–343 K). After every charging, the circuit was opened for 5 min.

The phases of the alloy powders were determined by X-ray diffraction (XRD) using a Rigaku D/max 2500PC powder diffractometer with Cu Kα radiation, and the surface morphology was examined by using scanning electron microscopy (SEM) JSM-5600. The electrochemical impedance spectroscopy (EIS) analysis was executed on a Solartron 1287 Potentiostat/Galvanostat and a Solartron 1255 frequency response analyzer with Z-POLT software. The electrodes were all tested at the steady state 10% depth of discharge (DOD) after different cycles at 323 K, and the frequency range was from 0.1 Hz to 1 MHz.

3. Results and discussion

3.1. Structure characteristics

Fig. 1 shows XRD patterns of mechanical alloyed (MAed) and annealed $Ti_{45}Zr_{35}Ni_{17}Cu_3$ powders. The MAed powders showed no sharp peak in its diffraction pattern and exhibited a broad diffuse peak at around 30–45°, which indicates that the specimen is an amorphous alloy. The powders annealed at 855 K for 30 min showed a single I-phase. The prominent I-phase is indexed following the scheme originally proposed by literature [14]. Takasaki et al. [9] have reported that the $Ti_{45}Zr_{38}Ni_{17}$ powders obtained by mechanical alloying and subsequent annealing contained I-phase and a small amount of Ti_2Ni-type crystal phase. This result indicates that the forming ability of the I-phase has been improved by adding Cu.

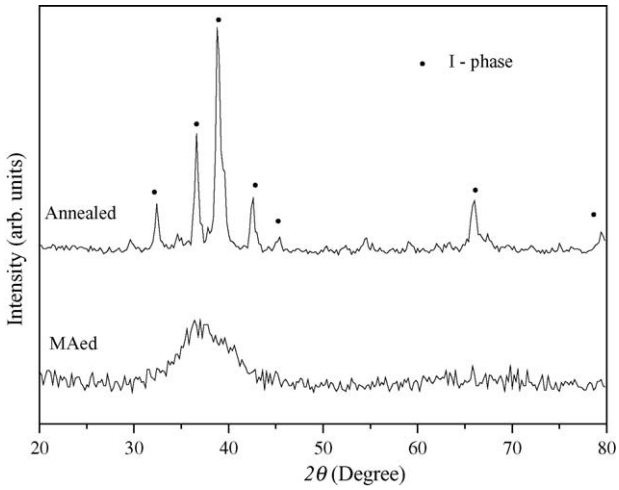

Fig. 1. XRD patterns of MAed and annealed $Ti_{45}Zr_{35}Ni_{17}Cu_3$ powders.

3.2. Maximum discharge capacity at different temperatures

Maximum discharge capacities (C_{max}) of the $Ti_{45}Zr_{35}Ni_{17}Cu_3$ amorphous and I-phase alloy electrodes at different temperatures (303, 313, 323, 333 and 343 K) are depicted in Fig. 2. It can be seen that the C_{max} of the amorphous and I-phase alloy electrodes increase with increasing temperature, and the C_{max} values are 86 and 76 mAh g^{-1} at 303 K, and 329 and 312 mAh g^{-1} at 343 K, respectively.

In most transition metal alloys, the hydrogen prefers the tetrahedral coordinated sites. The most I-phase showing the rotation

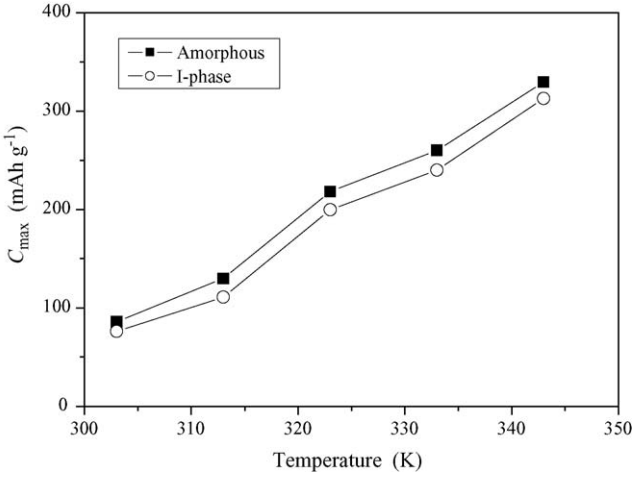

Fig. 2. The C_{max} of amorphous and I-phase $Ti_{45}Zr_{35}Ni_{17}Cu_3$ alloy electrodes at different temperatures.

symmetry of the icosahedral point group is likely dominated by local tetrahedral order. The amorphous alloy has similar local atomic structure to the I-phase alloy [15]. The dominance of polytetrahedral order is the origin for absorbing a large amount of hydrogen for the amorphous and I-phase alloy. The theoretical capacity of the Ti–Zr–Ni I-phase is 795 mAh g^{-1} [10]. However, the C_{max} values of $Ti_{45}Zr_{35}Ni_{17}Cu_3$ amorphous and I-phase alloy electrodes are only 86 and 76 mAh g^{-1} at 303 K. Besides the high hydrogen storage ability, the C_{max} values are related to the stability of hydride and electrochemical kinetics. Ti and Zr have significant negative enthalpy changes during hydrogenation and have a strong affinity with hydrogen [16]. The hydrides of amorphous and I-phase $Ti_{45}Zr_{35}Ni_{17}Cu_3$ alloys are difficult to dissociate at 303 K due to the high proportion of Ti and Zr. The equilibrium pressure of hydrogen increases with the increase of temperature, as a result, the stability of the hydride decreased, the hydrogen stored in the alloy easily desorbs from the alloy, and so the discharge capacities of two alloys increase with the increase of temperature. Meanwhile, the electrochemical reaction is controlled by the charge-transfer process on alloy surface and the mass transfer process in the bulk alloy [17]. The charge-transfer resistance decreases and the hydrogen diffusion coefficient increase with increasing temperature, which benefits to the increase of the discharge capacity. The C_{max} values of amorphous and I-phase alloys are 329 and 312 mAh g^{-1}. However, the C_{max} values are still much lower than the theoretical capacity, which may be ascribed to considerable stability of the hydride.

The discharge capacity of $Ti_{45}Zr_{35}Ni_{17}Cu_3$ amorphous alloy electrode is higher than that of I-phase alloy electrode at different temperatures, which results primarily from two factors: large amounts of special defects in the amorphous alloy obtained by mechanical alloying benefit to the diffusion of hydrogen in the alloy and improve the discharge property. In addition, according to the adsorption PCT curves at 523 K shown in Fig. 3, the plateau pressure for I-phase alloy is obviously lower than that for amorphous alloy. This indicates that the stability of I-phase alloy hydride is higher than that of the amorphous alloy hydride. Takasaki and Kelton [18] have investigated the site energy for hydrogen in the $Ti_{45}Zr_{38}Ni_{17}$ amorphous and I-phase alloy with PCT curves, and pointed out the site energy for hydrogen in the I-phase alloy is lower than that in the amorphous alloy. Thus, it is reasonable to consider that hydrogen atoms in the $Ti_{45}Zr_{35}Ni_{17}Cu_3$ I-phase alloy are more strongly bound than those in the amorphous alloy. The stronger bound of hydrogen in the I-phase alloy does not benefit to hydrogen desorption.

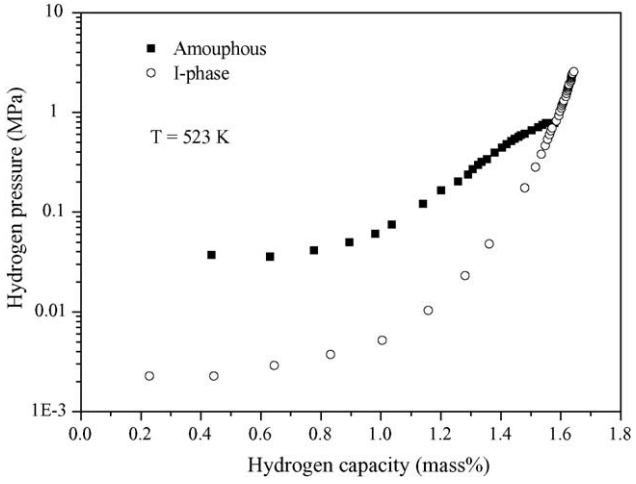

Fig. 3. Adsorption PCT for amorphous and I-phase $Ti_{45}Zr_{35}Ni_{17}Cu_3$ powders.

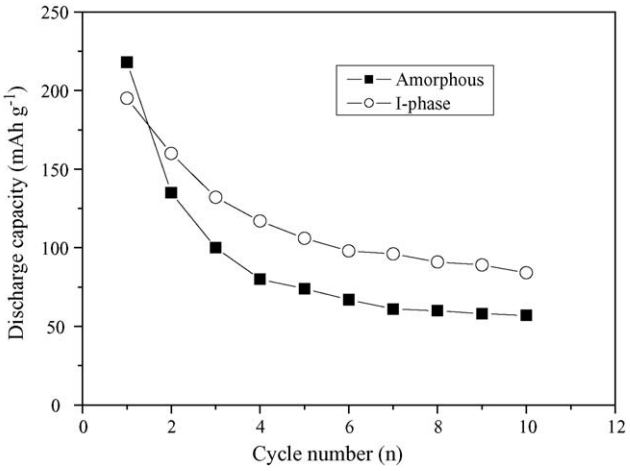

Fig. 4. The discharge capacity vs. cycle number for amorphous and I-phase $Ti_{45}Zr_{35}Ni_{17}Cu_3$ alloy electrodes at 323 K.

3.3. Cycle stability

Fig. 4 shows the discharge capacity versus cycle number for amorphous and I-phase $Ti_{45}Zr_{35}Ni_{17}Cu_3$ alloy at 323 K. For two alloy electrodes, no activation period is observed during cycle. C_{max} values are obtained at first electrochemical charge/discharge cycle, which indicates that two electrodes possess good activation at 323 K. The discharge capacity decreases distinctly with the increase of cycle number. The discharge capacities of amorphous and I-phase alloy electrodes are 57 and 84 mAh g^{-1} at 10th cycle, respectively, which have the maximum C_{max} value (1st cycle) of 26.1 and 44.2%, and the decreasing amount of discharge capacity of the I-phase alloy electrode is smaller than that of the amorphous alloy electrode.

3.4. Mechanism of the discharge capacity loss of I-phase alloy electrode

Fig. 5 shows XRD patterns of $Ti_{45}Zr_{35}Ni_{17}Cu_3$ I-phase alloy electrode after different cycles. It can be seen that I-phase is still retained after different charge/discharge cycles, which indicates that I-phase is stable and the similar hydride is formed during the charge/discharge cycles. Compared with the peaks corresponding to I-phase before cycle, the peaks shift to smaller angle after one cycle, resulting from an expansion of the lattice. This indicates that the alloy hydride remains, and does not release all the hydrogen absorbed at the first charging process. Meanwhile, the intensity of diffraction peaks decrease and the diffraction peaks broaden with the increase of cycle number, which may be due to strain in the lattice and refinement of crystal grains caused

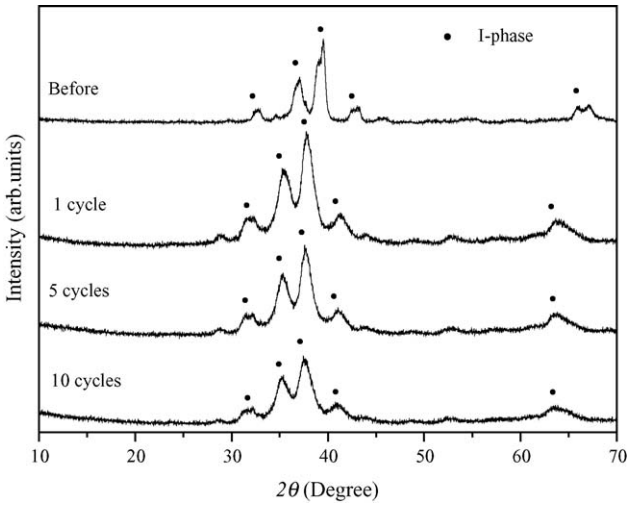

Fig. 5. XRD patterns of I-phase $Ti_{45}Zr_{35}Ni_{17}Cu_3$ alloy electrode after different cycles.

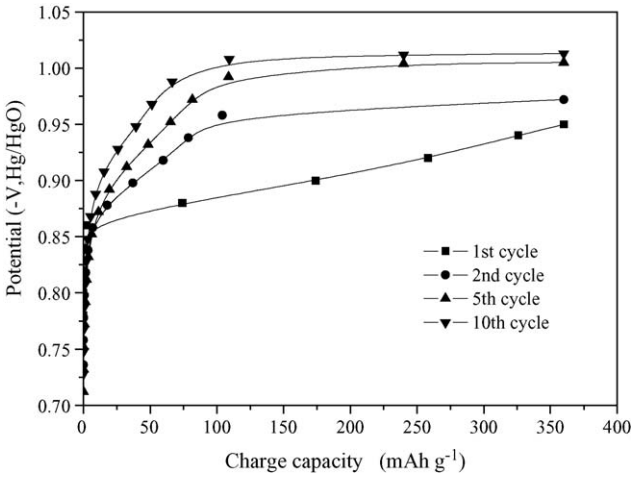

Fig. 7. Charging curves of I-phase $Ti_{45}Zr_{35}Ni_{17}Cu_3$ alloy electrode at different cycles.

by charge/discharge cycle. After 1 cycle, some oxide films may have formed on the alloy surface. However, the peaks corresponding to the oxide cannot be found, which results from that the amount of oxide is too small to be detected by XRD.

Fig. 6 shows electrochemical impedance spectra of $Ti_{45}Zr_{35}Ni_{17}Cu_3$ I-phase alloy electrode at the 10% DOD after different cycles. It can be seen that each spectrum consists of two semicircles and a straight line. According to the analysis of literature [19], the larger semicircle in the lower frequency region is ascribed to the charge-transfer resistance of the alloy surface, and the radius of the semicircle increases with the increase of cycle number, indicating that the charge-transfer resistance increases with the increase of cycle number. This is caused by the surface degradation, and during charge/discharge cycles, the alloy are gradually oxidized due to the contact with the alkaline electrolyte, and an oxide film is formed and grows in thickness, which decreased the electro-catalytic activity on the alloy surface [20].

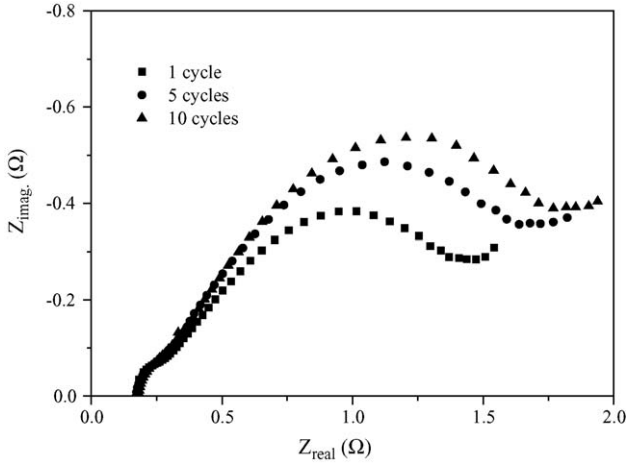

Fig. 6. Electrochemical impedance spectra of I-phase $Ti_{45}Zr_{35}Ni_{17}Cu_3$ alloy electrode at 10% DOD.

Fig. 7 shows charging curves of $Ti_{45}Zr_{35}Ni_{17}Cu_3$ I-phase alloy electrode at different cycles. Comparing the charging curves between the first and second cycles, a poor acceptance capacity is observed at the second cycle. This indicates that the hydride remains quite stable and does only release a part of the hydrogen absorbed at the first charging process, which is in agreement with the results of XRD. The potential of charging plateau increased and the charge efficiency of electrode decreases with the increase of cycle number, which may be resulted from the increase of the charge-transfer resistance on the alloy surface.

Fig. 8 shows SEM images of $Ti_{45}Zr_{35}Ni_{17}Cu_3$ I-phase alloy after different cycles. It can be seen the alloy particles are pulverized and particle size becomes smaller with the increase of cycle number. The particle size decreases from approximate 50 μm before cycle to approximate 5 μm after 10 cycles. The pulverization of alloy particles is due to the cell volume expansion and contraction during charging/discharging cycle.

I-phase is stable during charge/discharge cycle, and the discharge capacity degradation of the electrode results primarily from two following factors: the surface oxide is formed easily during charge/discharge cycles in the Ti-based alloy electrode [21]. At the initial charge/discharge stage, the film is thin, and then becomes thick with increasing cycle number, which leads to the increase of the charge-transfer resistance during the electrochemical hydrogenation reaction. This degrades the charge efficiency of the electrode, which can be confirmed by the results shown in Fig. 7. Meanwhile, a large charge-transfer resistance in the electrode also results in a higher anodic potential, which causes the electrode potential to drop rapidly to the cut-off potential and leads to the decrease of the discharge efficiency [22], suggesting the oxide film leads to the loss of discharge capacity. The lattice expansion of Ti–Zr–Ni quasicrystal is anisotropic with hydrogenation, which is due to the tendency of the H to site near the Ti and Zr atoms [23]. The recovery of lattice is difficult during hydrogen desorption. This expansion and contraction during charge/discharge cycle result in the pulverization of particles and produce fresh surface, which is confirmed by the

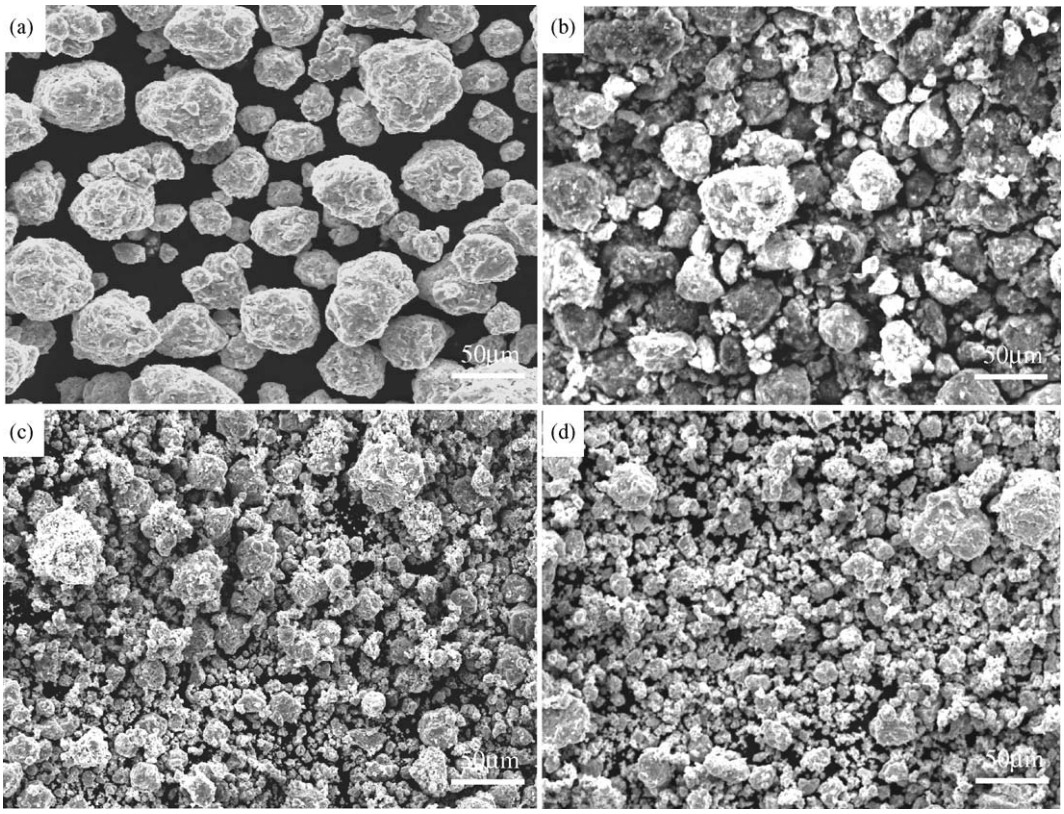

Fig. 8. SEM images of I-phase $Ti_{45}Zr_{35}Ni_{17}Cu_3$ alloy electrode after different cycles. Before cycle, (b), (c) and (d) are 1, 5 and 10 cycles, respectively.

results shown in Fig. 8. As a result, more fresh surface is exposed directly to the alkaline electrolyte, and then the active components of alloy are oxidized, which leads to the decrease of the discharge capacity.

3.5. Mechanism of the discharge capacity loss of amorphous alloy electrode

Fig. 9 shows XRD patterns of $Ti_{45}Zr_{35}Ni_{17}Cu_3$ amorphous alloy electrode after different cycles. It can be observed that

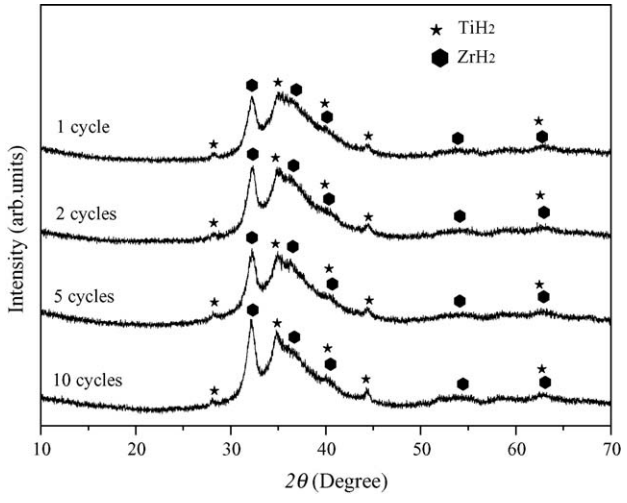

Fig. 9. XRD patterns of amorphous $Ti_{45}Zr_{35}Ni_{17}Cu_3$ alloy electrode after different cycles.

TiH_2 and ZrH_2 hydrides are formed after first electrochemical cycle, which is ascribed to the decomposition of partial amorphous phase during first charge/discharge process. This indicates that amorphous phase is not stable on electrochemical cycling. The hydride for amorphous electrode is different from that for I-phase electrode, which is attributed to the different structure between amorphous phase and I-phase. Moreover, the intensities of the peaks corresponding to the hydrides are gradually strengthened with increasing cycle number. This indicates the amount of the hydrides increase. That is to say, the amount of the amorphous phase in the alloy electrode decreases with the increase of the cycle number, which will lead to the decrease of the discharge capacity. Meanwhile, the increase of the charge-transfer resistance and the pulverization of alloy particle are observed for the amorphous alloy electrode. Thus, the loss of discharge capacity results from three factors: the formation of stable TiH_2 and ZrH_2 hydrides, the increase of the charge-transfer resistance and the pulverization of alloy particles.

4. Conclusions

$Ti_{45}Zr_{35}Ni_{17}Cu_3$ amorphous and single I-phase powders were synthesized by mechanical alloying and subsequent annealing at 855 K, respectively. At 303 K, the C_{max} values of amorphous and I-phase alloy electrode are 86 and 76 mAh g^{-1}, respectively, and the C_{max} values increase with increasing temperature, at 343 K, the C_{max} values are 329 and 312 mAh g^{-1}, respectively. In the case of the I-phase alloy electrode, I-phase is stable during the charge/discharge cycle. The reasons of

discharge capacity loss are the increase of the charge-transfer resistance for the formation of surface oxide film and the pulverization of alloy particles. The amorphous phase is not stable, the TiH_2 and ZrH_2 hydrides are formed during charge/discharge cycle, and the amount of hydride increases with increasing cycle number. The formation of the stable hydride, the increase of the charge-transfer resistance and the pulverization of alloy particles should be considered for the discharge capacity loss of the amorphous phase.

Acknowledgments

This work is supported by National Natural Science Foundations of China (50571094) and Scientific Research Foundation for the Returned Overseas Chinese Scholars, State Education Ministry. We are grateful to Prof. Liquan Li and Mr. Dongming Liu of the Nanjing University of Technology for pressure-composition isotherm measurement.

References

[1] K. Hong, J. Alloys Compd. 321 (2001) 307–313.
[2] A.P. Tsai, A. Niikura, K. Aoki, T. Masumoto, J. Alloys Compd. 253–254 (1997) 90–93.
[3] J.Y. Kim, P.C. Gibbons, K.F. Kelton, J. Alloys Compd. 266 (1998) 311–317.
[4] A. Sadoc, J.P. Itie, A. Polian, J.Y. Kim, K.F. Kelton, Mater. Sci. Eng. A 294–296 (2000) 804–805.
[5] D. Zander, H. Leptien, U. Koster, N. Eliaz, D. Eliezer, J. Non-Cryst. Solids 250–252 (1999) 893–897.
[6] A. Gebert, N. Ismail, U. Wolff, M. Uhlemann, J. Eckert, L. Schultz, Intermetallics 10 (2002) 1207–1213.
[7] R.M. Stroud, A.M. Viano, P.C. Gibbons, K.F. Kelton, Appl. Phys. Lett. 69 (1996) 2998–3000.
[8] A.M. Viano, R.M. Stroud, P.C. Gibbons, A. McDowell, M.S. Conradi, K.F. Kelton, Phys. Rev. B: Rapid Commun. 51 (1995) 12026–12029.
[9] A. Takasaki, V.T. Huett, K.F. Kelton, J. Non-Cryst. Solids 334–335 (2004) 457–460.
[10] E.H. Majzoub, J.Y. Kim, R.G. Hennig, K.F. Kelton, P.C. Gibbons, W.B. Yelon, Mater. Sci. Eng. A 294–296 (2000) 108–111.
[11] L. Wang, C. Li, A. Inoue, Mater. Trans. 42 (2001) 528–531.
[12] L. Wang, A. Inoue, Mater. Trans. 42 (2001) 2637–2640.
[13] L. Wang, L. Ma, C. Ma, A. Inoue, J. Alloys Compd. 361 (2003) 234–240.
[14] P. Bancel, P. Heiney, P. Stephens, A. Goldman, P. Horn, Phys. Rev. Lett. 54 (1985) 2422–2425.
[15] K.F. Kelton, Mater. Sci. Eng. A 375–377 (2004) 31–37.
[16] X. Guo, D. Lonzguine, S. Yamaura, L. Ma, W. Sun, M. Hasegawa, A. Inoue, Mater. Sci. Eng. A 133 (1991) 312–315.
[17] M. Geng, F. Feng, S.A. Gamboa, P.J. Sebastian, A.J. Matchett, D.O. Nothowood, J. Power Sources 96 (2001) 90–93.
[18] A. Takasaki, K.F. Kelton, J. Alloys Compd. 347 (2002) 295–300.
[19] N. Kuriyama, T. Sakai, H. Miyamura, I. Uehara, H. Ishikawa, T. Iwasaki, J. Alloys Compd. 202 (1993) 183–197.
[20] Y.F. Liu, H.G. Pan, Y.J. Yue, X.F. Wu, N. Chen, Y.Q. Lei, J. Alloys Compd. 395 (2005) 291–299.
[21] H.H. Lee, K.Y. Lee, J.Y. Lee, J. Alloys Compd. 253–254 (1997) 601–604.
[22] X.G. Yang, Y.Q. lei, K.Y. Shu, G.F. Lin, Q.A. Zhang, W.K. Zhang, X.B. Zhang, G.L. Lu, Q.D. Wang, J. Alloys Compd. 293–295 (1999) 632–636.
[23] A. Sadoc, J.Y. Kim, K.F. Keloton, Mater. Sci. Eng. A 294–296 (2000) 348–350.